Current Biology 23, 2051–2057, October 21, 2013 ©2013 Elsevier Ltd All rights reserved http://dx.doi.org/10.1016/j.cub.2013.08.043

Report

Budding Yeast Escape Commitment to the Phosphate Starvation Program Using Gene Expression Noise

Noam Vardi,[1] Sagi Levy,[1] Michael Assaf,[2] Miri Carmi,[1] and Naama Barkai[1,*]
[1]Department of Molecular Genetics, Weizmann Institute of Science, Rehovot 7610001, Israel
[2]Racah Institute of Physics, Hebrew University of Jerusalem, Jerusalem 91904, Israel

Summary

Cells must rapidly adapt to changes in nutrient availability. In budding yeast, limitation of phosphate rapidly induces the expression of the Pho regulon genes [1–4]. This starvation program depends on the transcription factor Pho4, which translocates to the nucleus within minutes when cells are transferred to a low-phosphate medium [5]. Contrasting its rapid induction, we report that the Pho regulon can remain induced for dozens of generations in cells transferred back to high phosphate levels. For example, about 40% of the cells that were starved for 2 hr maintained *PHO4*-dependent expression for over eleven generations of growing in high phosphate. This commitment to activation of the Pho regulon depends on two feedback loops that reduce internal phosphate, one through induction of the *PHM1-4* genes that increase phosphate storage in the vacuoles and the second by induction of *SPL2*, which reduces incoming flux by inhibiting low-affinity transporters. Noise in *SPL2* expression allows stochastic repression of the Pho regulon in committed cells growing at high phosphate, as we demonstrate using a novel method, DAmP multiple copy array (DaMCA), that reduces intrinsic noise in gene expression while maintaining mean abundance. Commitment is an integral part of the dual-transporter motif that helps cells prepare for nutrient depletion.

Results and Discussion

The molecular circuit that activates *PHO4* is well studied. Analyzing the dynamics of this circuit, we predicted that the entry of cells into phosphate starvation will include a transient phase of commitment (Figures 1A and 1B). By definition, committed cells will not respond to phosphate replenishment and will maintain the Pho regulon active for many generations of growth in high phosphate. This commitment phase was predicted based on two properties of the circuit, which are common to many nutrient homeostasis pathways. First, the cells monitor the internal (rather than external) nutrient levels [7–9]. Second, when phosphate is beginning to be depleted, the cells induce high-affinity transporters as part of the Pho regulon [10].

To see why commitment is expected, consider the phosphate influx into the cell as phosphate is gradually being depleted from the media. Since phosphate influx in high phosphate concentration depends on the low-affinity transporters, phosphate limitation will begin to be sensed when phosphate levels become comparable to the low-affinity transporters' dissociation constant, $K_d^{\text{low affinity}}$ (Figure 1A) [11, 12]. At this stage, the Pho regulon will be induced, resulting in the upregulation of high-affinity transporters and downregulation of the low-affinity ones. The phosphate influx will therefore become dependent on the high-affinity transporters alone, which at this point work at maximal velocity, returning the phosphate influx back to its maximum level. Maintaining the starvation program induced at intermediate phosphate therefore necessitates some positive feedback to maintain Pho4p active despite the high phosphate influx. Further, replenishing phosphate at this stage will not be sensed by the cells, as it will not increase phosphate uptake (Figure 1B). We therefore predicted that if phosphate is replenished when cells are in intermediate phosphate, the starvation program will remain active. Only when phosphate levels are reduced further, to a level that is comparable to the dissociation constant of the high-affinity transporters, will the cells be able to activate a secondary response to destabilize commitment and to downregulate the Pho regulon immediately upon phosphate replenishment (Figure 1A). A similar design, with a positive feedback loop (commitment) occurring at a first threshold following a negative feedback loop inactivating the commitment at a second threshold, was recently implicated in the budding yeast cell cycle [13].

Our initial observations in batch culture indicated that cells indeed become committed. Studies in batch cultures are limited, however, since phosphate levels are depleted while cells are growing, making it difficult to maintain controlled conditions. We reasoned that steady-state cultures may be better suited for examining commitment since phosphate conditions can be precisely controlled and monitored. We grew cells in a chemostat at varying phosphate levels and monitored the induction of the starvation program using the *PHO4*-dependent *PHO84pr*-yellow fluorescent protein (YFP) reporter. The reporter was induced in most cells when phosphate levels in the chemostat decreased to below 0.4 mM (see Figure S1A available online), significantly above the levels in which phosphate became growth limiting (below 5 μM, our detection limit).

Next, we replenished phosphate and monitored the cells' response. Our analysis predicted that deeply starved cells will downregulate the starvation program immediately upon phosphate replenishment. In contrast, cells subject to less severe limitation were predicted to be committed and therefore to maintain the starvation program active also after phosphate is added to the medium. When phosphate is the limiting factor in the chemostat, the extent of starvation is determined by the dilution rate [14]. Indeed, lowering the dilution rate from d = 0.3 [1/hr] to d = 0.1 [1/hr] increased reporter expression, indicating that cells are more deeply starved (Figures S1B and S1C). We replenished phosphate by switching the cells back to a high-phosphate medium (7.3 mM). The deeply starved cells (d = 0.1 [1/hr]) downregulated reporter expression almost immediately (Figure 1D; Figure S1D). In sharp contrast, cells at intermediate starvation (d = 0.3 [1/hr]) reduced reporter expression only slightly, to its levels at induced conditions, which are not yet phosphate limiting, and subsequently maintained this induced expression for dozens of generations in rich medium (Figures 1C and 1D; Figure S1E). Gene expression profiling confirmed that reporter induction mirrors the induction of the full Pho regulon (Figure 1E). Diploid and triploid cells maintained

*Correspondence: naama.barkai@weizmann.ac.il

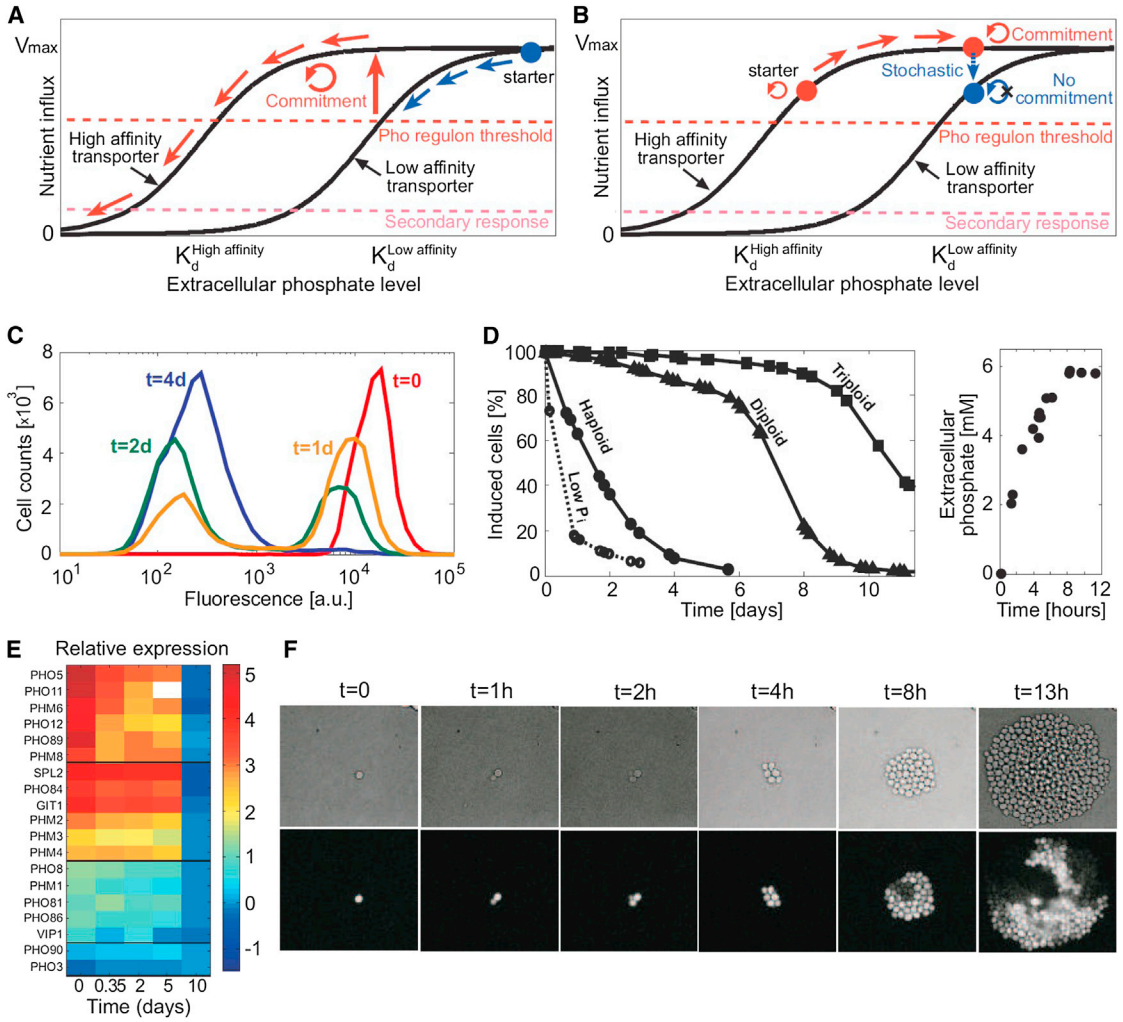

Figure 1. Dual Transporter System Entails Commitment

(A) Activation of the phosphate starvation response upon phosphate depletion: the Pho regulon is induced as part of the starvation program when extracellular phosphate levels decrease to below the dissociation constant of the low-affinity transporter $\sim K_d^{low\ affinity}$ ($\sim$220 μM, blue arrows). This induction increases phosphate uptake back to its maximal velocity due to the increased expression of the high-affinity transporter Pho84p (red arrow). A positive feedback is therefore required to stabilize the starvation program in this regime.

(B) Response to phosphate replenishment: since Pho84p works at maximal velocity in intermediate phosphate levels, the incoming flux will not change if phosphate is now replenished (red arrows). The cells are therefore predicted to maintain the starvation response induced even if phosphate is replenished. Escape from commitment may follow a stochastic event that destabilizes the feedback loop entailing commitment (dotted blue arrow). Note that when extracellular phosphate is decreased further to below the dissociation constant of the high-affinity transporter $K_d^{high\ affinity}$, cells may initiate a secondary response that could destabilize the feedback loop underlying commitment. Phosphate influx was modeled as a Hill curve with parameters taken from [6]: $K_d^{low\ affinity} \sim 220\ \mu M$,. $K_d^{high\ affinity} \sim 9\ \mu M$, and comparable maximal velocity of the two transporter types.

(C) Single-cell distribution of the *PHO84pr*-yellow fluorescent protein (YFP) reporter at different times following phosphate replenishment. Cells were grown in a chemostat at a dilution rate D = 0.3 hr^{-1} and phosphate feeding levels P_{feed} = 0.3 mM. The cells were allowed to reach steady state and transferred to medium with high phosphate (7.3 mM).

(D) Slow decrease in the fraction of induced cells: the experiment was performed as above, for haploid cells pregrown in low phosphate (D = 0.1 hr^{-1}, P_{feed} = 0.3 mM) and for haploids, diploids, and triploid cells pregrown in intermediate phosphate (D = 0.3 hr^{-1}, P_{feed} = 0.3 mM). The right panel shows the level of phosphate in the chemostat after transfer to a feeding medium with high phosphate (7.3 mM). Note that in contrast to this slow and stochastic dynamics, in which some cells remain induced for $\sim$40 generations after the transfer to high Pi, reporter activation upon transfer from high- to low-phosphate concentration was fast and synchronous, approximately three generations' time until full induction in the entire population (Figure S1F).

(E) Slow downregulation of the Pho regulon: gene expression was profiled at different time points after phosphate replenishment. Expression levels are shown as log2-ratios, with reference taken 10 days after transfer. Data correspond to diploids shown in (B).

(F) Stochastic downregulation *PHO84*pr-YFP reporter: committed cells (as in D) were transferred from the chemostat to a phosphate-rich agar plate (7.3 mM) and followed using fluorescence video microscopy. The upper and lower rows correspond to bright-field and fluorescence images, respectively. Additional movies, at 4 min time resolution, are available (http://barkai-serv.weizmann.ac.il/GroupPage/software.htm). Note that in contrast to this slow and stochastic dynamics, reporter activation upon transfer from high-phosphate chemostat to no-phosphate agar plate was fast and synchronous (Figure S1G).

the starvation program induced for a significantly longer time, likely resulting from ploidy-dependent reduction in stochastic variations (Figure 1D) [15]. Transferring cells from the chemostat to a high-phosphate agar plate for microscopic visualization revealed that individual cells downregulated reporter expression at stochastic times and transmitted the activation state to their

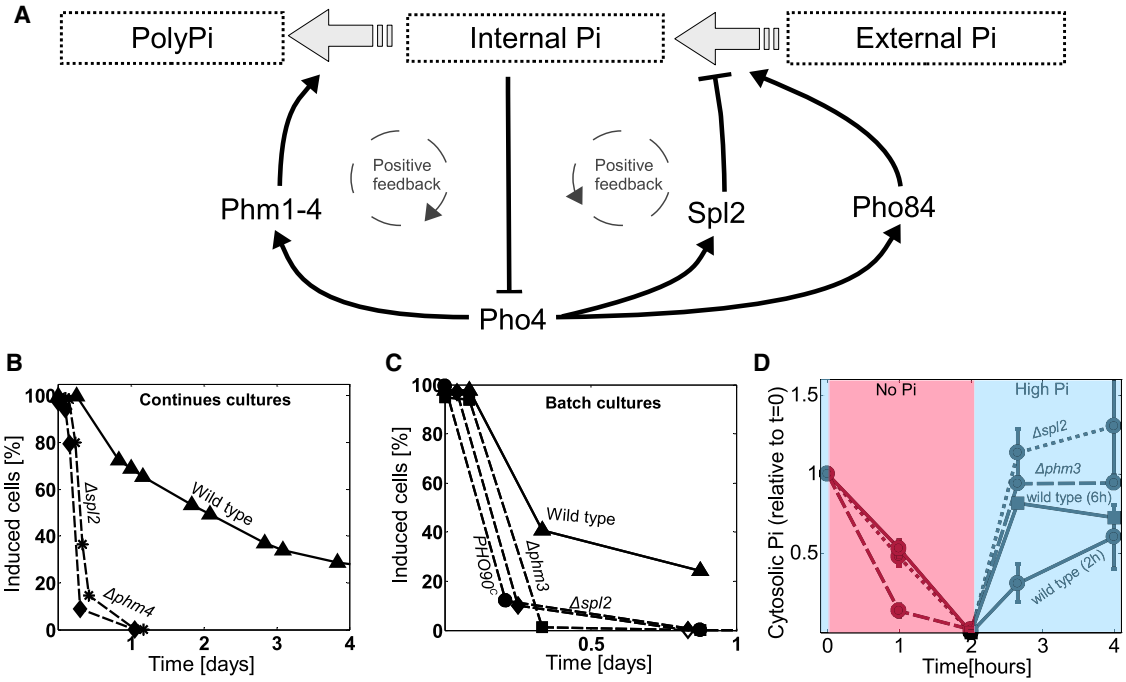

Figure 2. Loss of Commitment to the Phosphate Starvation Response

(A) Predicted feedback loop underlying commitment: Pho4p is the major transcription factor activating the starvation response and is activated at low internal Pi. As part of the starvation response, Pho4p upregulates *SPL2*, which inhibits the activity of the low-affinity transporters *phm1–4*, which mobilize Pi pools into storage as PolyPi and *PHO84*, a high-affinity Pi transporter.

(B) Loss of commitment in continuous cultures: wild-type (▲), *Δspl2* (◆), and *Δphm4* (*) cells were grown in a chemostats with intermediate phosphate levels (D = 0.3 hr^{-1}, P_{feed} = 0.3 mM), allowed to reach a steady state, and then transferred to medium with high phosphate (7.3 mM). *PHO84*pr-YFP distributions were measured at different times following the transfer and are shown in Figure S2D for *Δspl2*. Wild-type cells grown in similar conditions show bistable and slow deactivation of the starvation program (Figure 1C). A representative example of one out of two repeats is shown.

(C) Loss of commitment in batch cultures: wild-type (▲), *Δspl2* (◆), *Δphm3* (■), and $PHO90^C$ (●) cells growing in rich medium (high phosphate, 7.3 mM) were transferred into medium without phosphate for 2 hr and then transferred back to high-phosphate medium. *PHO84*pr-YFP distributions were measured at different times following the transfer and shown in Figure S2E. The $PHO90^C$ strain constitutively expresses *PHO90* under the *TDH3* promoter. A representative example of 1 out of 3 repeats is shown.

(D) Committed cells show low cytosolic Pi level: wild-type (solid line, circles), *Δspl2* (dotted line, circles), and *Δphm3* (dashed line, circles) cells were grown in high-Pi medium (7.3 mM, t = 0), washed twice with double-distilled water, transferred to medium containing no Pi for 2 hr, then washed again and transferred back to high-Pi medium (t = 2–4 hr). Wild-type was also grown for 6 hr in no-Pi medium and then transferred back to high Pi (solid line, squares, t = 2–4 hr). ^{31}P-nuclear magnetic resonance (NMR) spectra were measured in different time points during the experiment. Peaks were assigned according to the literature [17]. Cytosolic Pi levels were quantified as described in the Supplemental Experimental Procedures. An average of three (wild-type, three *Δspl2*), and two (*Δphm3*) repeats is shown; error bars represent SEs. One repeat is shown for wild-type after 6 hr in no Pi. See also Figure S2F.

progenies (Figure 1F). We conclude that while adapting to phosphate depletion, cells enter a phase of commitment, maintaining the Pho regulon induced even if phosphate is replenished.

We reasoned that commitment depends on the molecular circuit activated by Pho4p. Examining this circuit, we identified two positive feedbacks that could lock the cells in an induced state by reducing internal phosphate. The first loop is defined by the induction of the *PHM1*, *PHM2*, *PHM3*, and *PHM4* genes, whose protein products catalyze the conversion of cytoplasmic phosphate into vacuole-stored PolyP [2]. The second loop results from the induction of *SPL2*, whose protein product inhibits the activity of the low-affinity transporters, thereby reducing the phosphate influx [12, 16] (Figure 2A). Commitment was indeed lost in *Δphm3*, *Δphm4*, and *Δspl2* strains, confirming the involvement of those loops in the underlying mechanism (Figures 2B and 2C; Figures S2D and S2E). Further, if commitment depends on mechanisms that reduce the level of internal phosphate, it should be lost by increasing phosphate influx. Consistent with that, constitutive high expression of the low-affinity transporter *PHO90* abolished commitment (Figure 2C; Figure S2E).

We directly tested the hypothesis that committed cells maintain a low level of internal phosphate even after phosphate is replenished by monitoring internal phosphate using ^{31}P-nuclear magnetic resonance (^{31}P-NMR) spectroscopy. Those experiments were done in batch cultures, and we therefore first identified conditions that induce commitment (Figures S2A–S2C). Commitment was most apparent when cells were transferred to a no-Pi medium for 2 hr. Monitoring internal phosphate under those conditions, we found that uncommitted *Δphm3* or *Δspl2* cells increased internal phosphate level immediately upon transfer to rich media whereas wild-type cells showed a significantly slower increase with the internal phosphate remaining low for several hours of growing in phosphate-rich media (Figure 2D; Figure S2F). Note that wild-type cells that were grown in no-Pi medium for 6 hr also increased internal phosphate levels immediately upon transfer to rich media, consistent with the fact that only ~10% of the cells are committed after replenishing of phosphate (Figure 2D). Wild-type cells starved for 2 hr reached prestarved internal phosphate levels only after ~4 hr of growing in rich medium, at which point the culture contained a mixture of committed

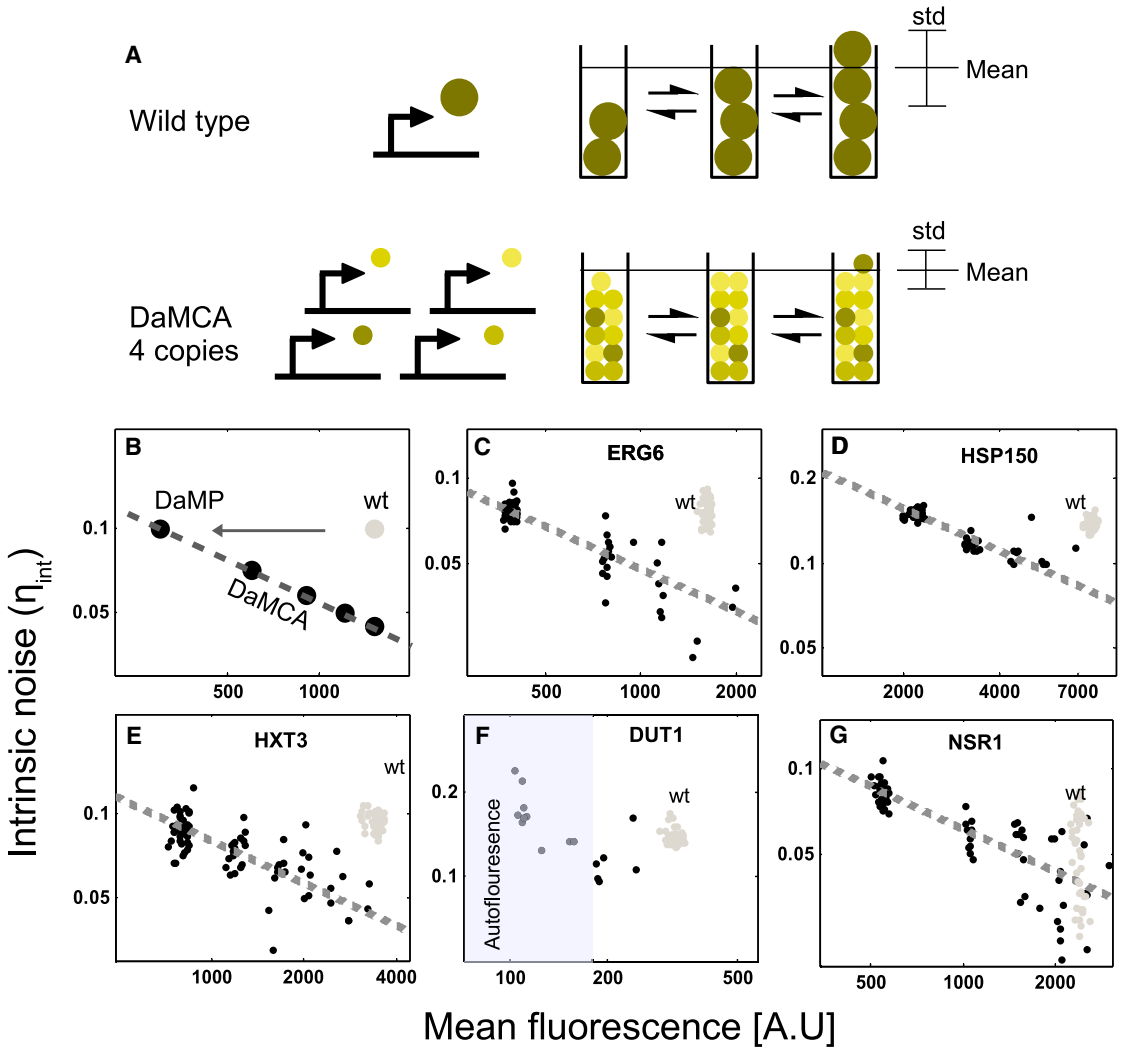

Figure 3. DaMCA Method Reduces Noise in Protein Expression

(A) Gene expression in a DaMCA gene: comparison between wild-type and DaMCA strains. In each transcription event the wild-type strain produces mRNA with half-life of τ and an average burst size of β (top panel). The DaMCA strain expresses four DaMP alleles, each one producing mRNA with a half-life of $\tau / 4$, and therefore with an average burst size of $\tau / 4$ (bottom panel). The steady-state concentration of mRNA will be the same in both strains, but the fluctuations due to random birth and death of molecules will be smaller in the DaMCA strain; therefore, expression noise (std / mean) will decrease.

(B) Predicted reduction of intrinsic noise expected in the DaMCA strains: models of gene expression noise predict that intrinsic noise level η_{int}^2 scales with mean abundance μ: $\eta_{int}^2 = \beta / \mu$ [21, 22] (dashed line). The DAmP allele reduces mean expression by reducing burst size (β); therefore, noise level is predicted to remain unchanged (gray dot compared to top black dot). Inserting multiple copies of the DAmP allele (black dots) will increase mean expression but will not change burst size. Therefore a DaMCA strain with the mean expression of the wild-type (lowest black dot) is predicted to have a lower noise than the wild-type.

(C–G) Noise decrease in different DaMCA strains: intrinsic noise versus mean expression measured for five different wild-type (gray dots) and DaMCA (black dots) strains corresponds to different promoters driving YFP expression. For each strain, total noise was measured as the normalized standard deviation over mean. Noise was decomposed into intrinsic and extrinsic components using the noise versus mean relation in each library following [28, 29]. Shown here are the intrinsic noise components. Total noise is shown in Figure S3B. Each dot corresponds to a different colony, averaged over two repeats. *dut1* DaMCA promoter expression is low, below autofluorescence, therefore extrinsic noise was calculated from tandem repeats of DUT1 promoter (see also Supplemental Experimental Procedures).

and uncommitted cells, making it difficult to distinguish the relative contribution of each population.

Noise in gene expression enables transition between stable states [18–20]. We hypothesized that the observed slow escape of cells from commitment is driven by expression noise (Figure 1B). To examine this hypothesis, we devised a general method called "DAmP multiple copy array" (DaMCA) that enables reducing intrinsic noise in gene expression while maintaining mean abundance. This method is based on the theoretical result that genes expressed at the same mean level, μ, can still display different intrinsic noise levels, η, depending on the average number of proteins made per each mRNA: $\eta^2 = \beta/\mu$. Here, β denotes the so-called "burst size," which is the average number of proteins made per stochastic transcription event. Clearly, β is proportional to the number of proteins made per each mRNA [21–25]. The DaMCA method reduces the burst size by destabilizing the mRNA through the insertion of an antibiotic marker immediately following the stop codon [26, 27]. It subsequently compensates for the reduction in mean abundance by integrating multiple gene copies transcribing this DAmP allele (Figures 3A and 3B; Figure S3A). Notably, this procedure generates a library of strains that

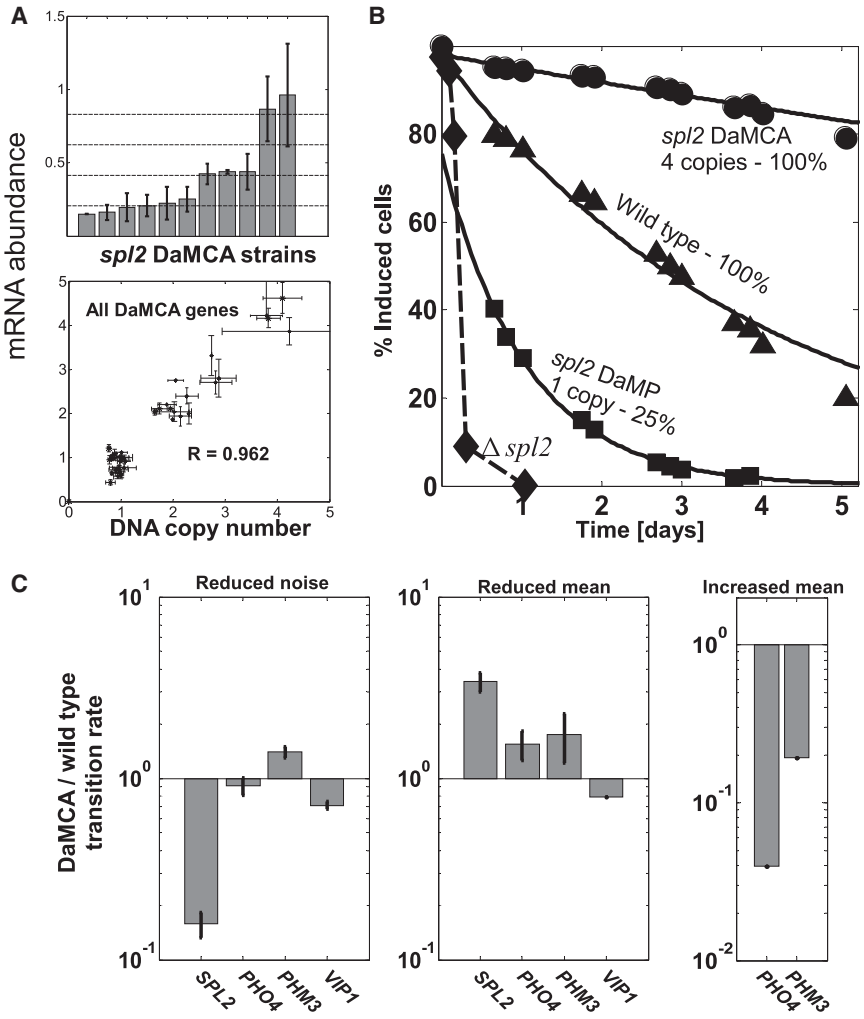

Figure 4. Escape from Commitment Depends on Intrinsic Noise in SPL2

(A) mRNA and DNA copy-number in different DaMCA strains: shown are the levels of *SPL2* mRNA transcript as well as the gene copy number for different genes in the different strains of the DaMCA library as measured by qPCR. Error bars are SEs.

(B) Escape rates depend on the mean level and on the noise in *SPL2* expression: *spl2*-DaMCA strains carrying the indicated number of *spl2*-DAmP alleles were analyzed for the rate by which they escape commitment. Chemostat assay was used as described in Figure 1D. The mean expression of each *spl2*-DAmP allele is 25% of the wild-type. The fraction of committed cells $N^{on}_{(t)}$ was fitted to an exponential decay model, $N^{on}_{(t)} = N^{on}_{(0)}e^{-\alpha t}$ (see also Experimental Procedures and Table S2). The *Δspl2* strain did not show commitment.

(C) Escape rate for different DaMCA strains: shown are the relative escape rates of the different DaMCA strains showing wild-type expression (left panel, $0.88 < \mu < 1.03$ of the wild-type mRNA abundance), low expression (middle panel, $0.25 < \mu < 0.5$ of the wild-type mRNA abundance), and high expression (right panel, $2 < \mu < 3$ fold of the wild-type mRNA abundance). Rates were obtained by fitting the experimental data to an exponential decay model as described above. Error bars represent SEs.

overexpress or underexpress the gene of interest by a defined amount measured by qPCR. Applying this method to different promoters driving YFP expression confirmed the expected reduction in intrinsic noise (Figures 3B–3G; Figures S3B and S3C).

We applied the DaMCA method to different components of the *PHO4* feedback circuit and measured the rate of escape from commitment. The *spl2*-DAmP allele reduced mRNA stability 4-fold. This reduction enhanced the rate by which cells escaped commitment, reducing the escape time from t = 84 ± 22 hr in the wild-type cells to t = 32 ± 9 hr in the strain expressing the *spl2*-DAmP allele (Figures 4A–4C). Introducing four copies of the DAmP allele retrieved wild-type mean expression, as verified by qPCR (Figure 4A). In this strain, escape rate was significantly reduced, with the typical escape time increasing to t = 628 ± 140 hr. Therefore, intrinsic noise in *SPL2* expression plays a key role in enabling escape from commitment. In contrast, for *PHM3*, where the DAmP allele reduced expression by 2-fold, recovering wild-type expression did not change the escape rate. Introducing four alleles, totaling a 2-fold increase in *PHM3* abundance, significantly stabilized commitment (Figure 4C; Figures S4A and S4B). Similar results were also observed when modulating the expression of the master regulator *PHO4*: commitment was greatly stabilized when *PHO4* abundance was increased, but escape rates were only moderately sensitive to 2-fold decrease in *PHO4* level and did not change in the DaMCA strain that retrieves wild-type mean abundance. (Figure 4C; Figures S4A and S4B). The data are therefore consistent with a model in which noise in *SPL2* expression drives escape from commitment: a stochastic reduction in *SPL2* levels transiently increases phosphate influx leading to *PHO4* inactivation, which is subsequently stabilized by the downregulation of *SPL2*, *PHM3*, and *PHM4* (Figure 2A; see mathematical model in Supplemental Experimental Procedures and in Figure S4C).

In summary, commitment is known to be important for cell differentiation and cell-cycle progression [13, 30, 31] but was not thought to play a role in the rapid adaptation of cells to the nutrient composition of their environment. We now identify commitment in budding yeast nutrient homeostasis. Further, our theoretical analysis suggests that commitment may be a general consequence of the "dual transporter motif" used by many nutrient homeostasis systems, in which cells monitor the internal nutrient levels and induce the high-affinity transporters as part of the starvation program. The dual transporter motif enables cells to prepare in advance of nutrient depletion [32], and the fact that it necessitates commitment suggests that it could not have been utilized in the absence of noise; indeed, in the deterministic case, cells would be trapped in a committed state and would not be able to downregulate the starvation program if nutrients were replenished during the commitment stage. Gene expression noise therefore plays an integral part in nutrient homeostasis, enabling computational designs that would not have been possible by the deterministic dynamics alone.

Experimental Procedures

Live Imaging Microscopy

Images of single-cell dynamics were collected by a high-throughput microscope system with fast laser [33] using a YFP filter set (Chroma, 41028) and a cooled electron-multiplying charge-coupled device camera (Andor iXon). Cells were maintained on the same focal plane by growing them in a 96-well plate below a thick agarose layer (Lonza).

Flow Cytometry

Fluorescence-activated cell sorting analysis of *PHO84*pr-YFP was done by a BD LSRII system (BD Biosciences). Flow cytometry was conducted with excitation at 488 nm and emission at 525 ± 25 nm for GFP samples. For mCherry markers, excitation was conducted at 594 nm and emission at 610 ± 10 nm.

qPCR

Cells were grown to OD = 0.2 and transferred for 2 hr to no-phosphate medium. Cells were harvested and frozen in liquid nitrogen; DNA and RNA were extracted using epicenter RNA purification kit and epicenter RNA purification kit respectively, and RNA was transcribed to cDNA using Sigma RT. cDNA and DNA levels measured relative to the wild-type using ACT1 as a reference (Lightcycler 480, Roche). Two biological repeats were averaged; error bars stand for SE.

Chemostat Experiments

Cells were grown in BioFlo 110 chemostats (New Brunswick Scientific) with the following parameters: dilution rate = 0.3 hr^{-1} or 0.1 hr^{-1}, chemostat working volume ~700 ml, temperature = 30°C, agitation speed = 500 RPM, air flux = 1 LPM. The pH was set on 5 by titration with NaOH (0.25 M). Note that in order to validate our results, cell samples were occasionally characterized under the microscope.

Calculating Transition Rates in Chemostat Experiments

Transition rate was calculated by fitting the experimental data to an exponential decay model, reflecting the stochastic nature of the process (see also Table S2). In order to neutralize experimental variability, the transition rates in each experiment were normalized with respect to a wild-type control that was monitored in the same experiment.

Accession Numbers

The microarray data reported in this paper are available in the Gene Expression Omnibus (GEO) database (http://www.ncbi.nlm.nih.gov/gds) under the accession numbers GSE50654, GSE50655, and GSE50656.

Supplemental Information

Supplemental Information includes four figures, four tables, Supplemental Experimental Procedures, and a supplemental spreadsheet and can be found with this article online at http://dx.doi.org/10.1016/j.cub.2013.08.043.

Acknowledgments

We thank S. Fialkov, S. Maizel, and L. Konstantinovski for technical help and G. Hornung, I. Soifer, and our lab members for helpful discussions. This work was supported by the ERC and by the Hellen and Martin Kimmel award for innovative investigations.

Received: December 25, 2012
Revised: July 9, 2013
Accepted: August 14, 2013
Published: October 3, 2013

References

1. Lenburg, M.E., and O'Shea, E.K. (1996). Signaling phosphate starvation. Trends Biochem. Sci. *21*, 383–387.
2. Ogawa, N., DeRisi, J., and Brown, P.O. (2000). New components of a system for phosphate accumulation and polyphosphate metabolism in Saccharomyces cerevisiae revealed by genomic expression analysis. Mol. Biol. Cell *11*, 4309–4321.
3. Oshima, Y. (1997). The phosphatase system in Saccharomyces cerevisiae. Genes Genet. Syst. *72*, 323–334.
4. Persson, B.L., Lagerstedt, J.O., Pratt, J.R., Pattison-Granberg, J., Lundh, K., Shokrollahzadeh, S., and Lundh, F. (2003). Regulation of phosphate acquisition in Saccharomyces cerevisiae. Curr. Genet. *43*, 225–244.
5. Kaffman, A., Rank, N.M., and O'Shea, E.K. (1998). Phosphorylation regulates association of the transcription factor Pho4 with its import receptor Pse1/Kap121. Genes Dev. *12*, 2673–2683.
6. Wykoff, D.D., and O'Shea, E.K. (2001). Phosphate transport and sensing in Saccharomyces cerevisiae. Genetics *159*, 1491–1499.
7. Auesukaree, C., Homma, T., Tochio, H., Shirakawa, M., Kaneko, Y., and Harashima, S. (2004). Intracellular phosphate serves as a signal for the regulation of the PHO pathway in Saccharomyces cerevisiae. J. Biol. Chem. *279*, 17289–17294.
8. Mouillon, J.M., and Persson, B.L. (2006). New aspects on phosphate sensing and signalling in Saccharomyces cerevisiae. FEMS Yeast Res. *6*, 171–176.
9. Lee, Y.S., Huang, K., Quiocho, F.A., and O'Shea, E.K. (2008). Molecular basis of cyclin-CDK-CKI regulation by reversible binding of an inositol pyrophosphate. Nat. Chem. Biol. *4*, 25–32.
10. Bun-Ya, M., Nishimura, M., Harashima, S., and Oshima, Y. (1991). The PHO84 gene of Saccharomyces cerevisiae encodes an inorganic phosphate transporter. Mol. Cell. Biol. *11*, 3229–3238.
11. Springer, M., Wykoff, D.D., Miller, N., and O'Shea, E.K. (2003). Partially phosphorylated Pho4 activates transcription of a subset of phosphate-responsive genes. PLoS Biol. *1*, E28.
12. Wykoff, D.D., Rizvi, A.H., Raser, J.M., Margolin, B., and O'Shea, E.K. (2007). Positive feedback regulates switching of phosphate transporters in S. cerevisiae. Mol. Cell *27*, 1005–1013.
13. Eser, U., Falleur-Fettig, M., Johnson, A., and Skotheim, J.M. (2011). Commitment to a cellular transition precedes genome-wide transcriptional change. Mol. Cell *43*, 515–527.
14. Segel, L.A. (1984). Modeling Dynamic Phenomena in Molecular and Cellular Biology (Cambridge: Cambridge University Press).
15. Di Talia, S., Skotheim, J.M., Bean, J.M., Siggia, E.D., and Cross, F.R. (2007). The effects of molecular noise and size control on variability in the budding yeast cell cycle. Nature *448*, 947–951.
16. Ghillebert, R., Swinnen, E., De Snijder, P., Smets, B., and Winderickx, J. (2011). Differential roles for the low-affinity phosphate transporters Pho87 and Pho90 in Saccharomyces cerevisiae. Biochem. J. *434*, 243–251.
17. Navon, G., Shulman, R.G., Yamane, T., Eccleshall, T.R., Lam, K.B., Baronofsky, J.J., and Marmur, J. (1979). Phosphorus-31 nuclear magnetic resonance studies of wild-type and glycolytic pathway mutants of Saccharomyces cerevisiae. Biochemistry *18*, 4487–4499.
18. Acar, M., Mettetal, J.T., and van Oudenaarden, A. (2008). Stochastic switching as a survival strategy in fluctuating environments. Nat. Genet. *40*, 471–475.
19. Kaufmann, B.B., Yang, Q., Mettetal, J.T., and van Oudenaarden, A. (2007). Heritable stochastic switching revealed by single-cell genealogy. PLoS Biol. *5*, e239.
20. Acar, M., Becskei, A., and van Oudenaarden, A. (2005). Enhancement of cellular memory by reducing stochastic transitions. Nature *435*, 228–232.
21. Thattai, M., and van Oudenaarden, A. (2001). Intrinsic noise in gene regulatory networks. Proc. Natl. Acad. Sci. USA *98*, 8614–8619.
22. Paulsson, J. (2004). Summing up the noise in gene networks. Nature *427*, 415–418.
23. Bar-Even, A., Paulsson, J., Maheshri, N., Carmi, M., O'Shea, E., Pilpel, Y., and Barkai, N. (2006). Noise in protein expression scales with natural protein abundance. Nat. Genet. *38*, 636–643.
24. Newman, J.R., Ghaemmaghami, S., Ihmels, J., Breslow, D.K., Noble, M., DeRisi, J.L., and Weissman, J.S. (2006). Single-cell proteomic analysis of S. cerevisiae reveals the architecture of biological noise. Nature *441*, 840–846.
25. Hornung, G., Bar-Ziv, R., Rosin, D., Tokuriki, N., Tawfik, D.S., Oren, M., and Barkai, N. (2012). Noise-mean relationship in mutated promoters. Genome Res. *22*, 2409–2417.
26. Muhlrad, D., and Parker, R. (1999). Aberrant mRNAs with extended 3′ UTRs are substrates for rapid degradation by mRNA surveillance. RNA *5*, 1299–1307.
27. Schuldiner, M., Collins, S.R., Thompson, N.J., Denic, V., Bhamidipati, A., Punna, T., Ihmels, J., Andrews, B., Boone, C., Greenblatt, J.F., et al. (2005). Exploration of the function and organization of the yeast early secretory pathway through an epistatic miniarray profile. Cell *123*, 507–519.

28. Stewart-Ornstein, J., Weissman, J.S., and El-Samad, H. (2012). Cellular noise regulons underlie fluctuations in Saccharomyces cerevisiae. Mol. Cell *45*, 483–493.
29. Volfson, D., Marciniak, J., Blake, W.J., Ostroff, N., Tsimring, L.S., and Hasty, J. (2006). Origins of extrinsic variability in eukaryotic gene expression. Nature *439*, 861–864.
30. Hartwell, L.H., Culotti, J., Pringle, J.R., and Reid, B.J. (1974). Genetic control of the cell division cycle in yeast. Science *183*, 46–51.
31. Doncic, A., Falleur-Fettig, M., and Skotheim, J.M. (2011). Distinct interactions select and maintain a specific cell fate. Mol. Cell *43*, 528–539.
32. Levy, S., Kafri, M., Carmi, M., and Barkai, N. (2011). The competitive advantage of a dual-transporter system. Science *334*, 1408–1412.
33. Paran, Y., Ilan, M., Kashman, Y., Goldstein, S., Liron, Y., Geiger, B., and Kam, Z. (2007). High-throughput screening of cellular features using high-resolution light-microscopy; application for profiling drug effects on cell adhesion. J. Struct. Biol. *158*, 233–243.